Dossier

This paper is a part of the hereunder thematic dossier published in OGST Journal, Vol. 67, No. 6, pp. 883-1039 and available online here

Cet article fait partie du dossier thématique ci-dessous publié dans la revue OGST, Vol. 67, n°6, pp. 883-1039 et téléchargeable ici

DOSSIER Edited by/Sous la direction de : **B. Bazin**

Challenges and New Approaches in EOR

Défis et nouvelles approches en EOR

Oil & Gas Science and Technology – Rev. IFP Energies nouvelles, Vol. 67 (2012), No. 6, pp. 883-1039

IFP Energies nouvelles

Oil & Gas Science and Technology – Rev. IFP Energies nouvelles, Vol. 67 (2012), No. 6, pp. 1029-1039

DOI: 10.2516/ogst/2012027

Dossier
Challenges and New Approaches in EOR
Défis et nouvelles approches en EOR

Evolution of Seismic Velocities in Heavy Oil Sand Reservoirs during Thermal Recovery Process

J.-F. Nauroy[1], D.H. Doan[1], N. Guy[1], A. Baroni[1], P. Delage[2] and M. Mainguy[3]

1 IFP Energies nouvelles, 1-4 avenue de Bois-Préau, 92852 Rueil-Malmaison Cedex - France
2 École des Ponts ParisTech, UMR Navier/CERMES, 6-8 Av. Blaise Pascal, 77455 Marne-la-Vallée Cedex 2 - France
3 TOTAL Office EB-181 CSTJF, Av. Larribau, 64018 Pau Cedex - France
e-mail: jean-francois.nauroy@ifpen.fr - doan_hong_47xf@yahoo.fr - nicolas.guy@ifpen.fr - axelle.baroni@ifpen.fr delage@cermes.enpc.fr - marc.mainguy@total.com

Résumé — Évolution des vitesses sismiques dans les réservoirs de sables bitumineux au cours des procédés de récupération thermique — Dans les procédés de récupération des huiles lourdes par méthodes thermiques, comme la stimulation cyclique par vapeur (CSS) ou le drainage par gravité assisté par vapeur (SAGD), l'injection de vapeur en continu entraîne des changements de liquide de pores, de pression interstitielle et de température dans la roche réservoir, qui est constituée le plus souvent de sable non consolidés ou faiblement consolidés. Ces changements à leur tour augmentent ou diminuent les contraintes effectives et modifient les propriétés élastiques des roches. Les procédés de récupération par méthodes thermiques mettent en œuvre des couplages complexes. Des campagnes de sismique 4D sont couramment effectuées pour suivre les zones affectées par la vapeur, mais leur interprétation est difficile. Elle est pourtant essentielle pour optimiser le développement du réservoir.

Des simulations numériques ont été réalisées sur un cas d'étude afin de fournir une estimation de l'évolution des pressions, températures, saturation des fluides interstitiels, contraintes et déformations dans toute zone située autour des puits injecteur et producteur.

L'approche de Ciz et Shapiro (2007) (*Geophysics* **72**, A75-A79) a été utilisée pour modéliser la dispersion de vitesse dans les sables bitumineux sous différentes conditions de température et de contrainte. Un bon accord a été trouvé entre les prédictions du modèle et certaines mesures de vitesse effectuées en laboratoire sur des échantillons de sables bitumineux Canadiens. Les résultats sont utiles pour mieux interpréter les données sismiques 4D afin de localiser la chambre à vapeur.

Abstract* — *Evolution of Seismic Velocities in Heavy Oil Sand Reservoirs during Thermal Recovery Process — *In thermally enhanced recovery processes like Cyclic Steam Stimulation (CSS) or Steam Assisted Gravity Drainage (SAGD), continuous steam injection entails changes in pore fluid, pore pressure and temperature in the rock reservoir, that are most often unconsolidated or weakly consolidated sandstones. This in turn increases or decreases the effective stresses and changes the elastic properties of the rocks. Thermally enhanced recovery processes give rise to complex couplings. 4D seismic surveys are currently conducted to delineate the steam-affected areas but the interpretation is difficult. However, it is essential for optimization of reservoir development.*

Numerical simulations have been carried out on a case study so as to provide an estimation of the evolution of pressure, temperature, pore fluid saturation, stress and strain in any zone located around the injector and producer wells.

*The approach of Ciz and Shapiro (*2007) (*Geophysics* **72**, A75-A79) *has been used to model the velocity dispersion in the oil sand mass under different conditions of temperature and stress. A good agreement*

has been found between these predictions and some laboratory velocity measurements carried out on samples of Canadian oil sand. Results appear to be useful to better interpret 4D seismic data in order to locate the steam chamber.

INTRODUCTION

Huge quantities of heavy oils (heavy oil, extra heavy oil and bitumen) are mainly trapped in unconsolidated sand and sandstone reservoirs in Western Canada and Eastern Venezuela basins. In thermally enhanced recovery processes like Cyclic Steam Stimulation (CSS) or Steam Assisted Gravity Drainage (SAGD), the injection of steam in oil sand deposits produces changes in temperature, pressures and pore fluid content. These changes obviously affect the elastic and seismic properties of the soil layers. Time-lapse 3D seismic (4D seismic) and other seismic technologies can be used to monitor the impact of these changes in unconsolidated sands or weakly consolidated sand reservoirs (Zhang *et al*., 2005; Nakayama *et al*., 2008; Tanaka *et al*., 2009). By comparing maps of seismic attributes (velocity, amplitude, attenuation, etc.) at different times, the continuous spatial distribution of heated reservoir zones can be approximately located. The purpose of seismic monitoring methods is to observe the visible changes of seismic attributes during the thermal process. These changes could be better understood from a combination of rock physics modeling and direct laboratory measurements.

Over the past three decades, several laboratory measurements of seismic properties (wave velocity and attenuation) of heavy oil sands have been published (Mraz *et al*., 1982; Nur *et al*., 1984; Tosaya *et al*., 1987; Wang and Nur, 1988, 1990; Wang *et al*., 1990; Eastwood, 1993; Kato *et al*., 2008). However, there is still a lack of clear understanding due, on the one hand, to well-known difficulties in obtaining representative samples of oil sands and on the other hand to the limits of testing systems that are generally designed for hard rock but not for unconsolidated oil sands. In addition, the application to field problems of laboratory results obtained with ultrasonic frequency is not obvious because of the wave dispersion that occurs in heavy oil sands.

Several attempts to model the properties of rock saturated with heavy oil have been made (Das and Batzle, 2008; Ciz *et al*., 2009). The difficulties are largely related to the viscoelastic behaviour of heavy oils. Heavy oils behave either like a quasi-solid at high frequencies and/or low temperature or like a viscous fluid at low frequencies and/or high temperature (Batzle *et al*., 2006b; Hinkle, 2008). Heavy oils have a non-negligible shear modulus that depends on both frequency and temperature and that allows propagation of shear waves. So, the physical characterization of rock saturated with heavy oil is different from that of rock saturated with conventional fluids with no shear modulus. It makes the standard poroelastic Biot-Gassmann approach (Biot, 1941; Gassmann, 1951) inapplicable (Ciz and Shapiro, 2007; Gurevich *et al*., 2008; Ciz *et al*., 2009). The generalization of the Biot-Gassmann equations originally made for porous rock saturated with an elastic material (Ciz and Shapiro, 2007) can be considered in a first attempt to model the seismic responses of heavy oil-saturated rocks. The feasibility of this approach in predicting the velocities of heavy oil sand was considered in this paper.

1 EVOLUTION OF PRESSURE, TEMPERATURE AND PORE FLUID SATURATION DURING SAGD

Coupled thermo-hydro-mechanical modeling of SAGD has been conducted at IFPEN (Lerat *et al*., 2010; Zandi, 2011), showing how the different fields (stress, pressure, temperature and steam) develop with respect to time. The results presented in this section have been obtained through a coupled simulation made by using the geometry and the parameters already presented by Zandi (2011). This simulation is based on an iterative coupling between a reservoir simulator (PumaFlow™) and a geomechanical simulator (ABAQUS™) in order to take into account the geomechanical effects on the porous volume and on the permeability changes of the reservoir. The iterative coupling has been done considering an implicit correction of the porous volume in the reservoir simulator that is driven the volume changes provided by the geomechanical simulator (Settari and Mourits, 1998; Longuemare *et al*., 2002). The convergence criterion relies on an analysis of the porous volume in both simulators and it requires a relative difference below 10^{-3} to be reached. The permeability considered in the reservoir simulator is linked with geomechanical strain considering the empirical relationship proposed by (Touhidi-Bagigni, 1998) that reads:

$$\ln \frac{k_1}{k_0} = \frac{c}{\varphi_0} \varepsilon_v \tag{1}$$

with k_1 the updated absolute permeability, k_0 the initial absolute permeability, ε_v the volumetric strain and c a constant. The values $c = 5$ and $c = 2$ are considered to match the vertical and horizontal permeability evolutions. In this simulation, a 20 meters thick (in the Z vertical direction) reservoir at a depth of 250 meters is modelled. The domain considered for the reservoir simulator is rectangular with a width of 147 meters (in the X direction) and a length of 500 meters

along the *Y*-axis of the well pair. The mesh used by the reservoir simulator in the *X-Z* plane is shown in Figure 1a. It contains only one grid block in the *Y* direction. The pair of wells is located at the centre of the domain and the injection well is 3.5 meters upper than the production well (see *Fig. 1a* where points *I* and *P* represent the position of the injection and production wells, respectively). The domain considered in the geomechanical model is built from the surface to a depth of 280 meters, including an underburden layer 10 meters thick. It should be noted that, in the geomechanical model, the displacements along the *Y* axis are blocked, corresponding to a plane strain condition. For simplicity, the rock response is considered linear elastic and isotropic. More information about the parameters considered has been given by Zandi (2011).

The simulations are performed over 1 500 days. The first 120 days correspond to the pre-heating of the zones surrounding both wells by circulating steam in order to reduce the oil viscosity and to create a hydraulic connection between them. Once pre-heating is finished, steam injection starts at a temperature of about 260°C. The steam injection and production rates are automatically controlled with a maximal pressure set to 5 MPa in the injection well and a minimum pressure of 0.5 MPa in the production well. Rates are automatically controlled based on the analysis of the temperature of each well. Rates are adjusted in order to keep the production well temperature between 20°C and 35°C, lower than the injection well temperature.

In the model associated with the reservoir simulator, fluids cannot flow through the boundaries. Heat losses by conduction through the upper and lower boundaries are taken into account by a simplified one-dimensional modeling of the overburden and underburden that is oriented in the vertical direction. In the geomechanical model, the horizontal displacements of lateral boundaries, as well as all the displacements of the lower boundary, are blocked.

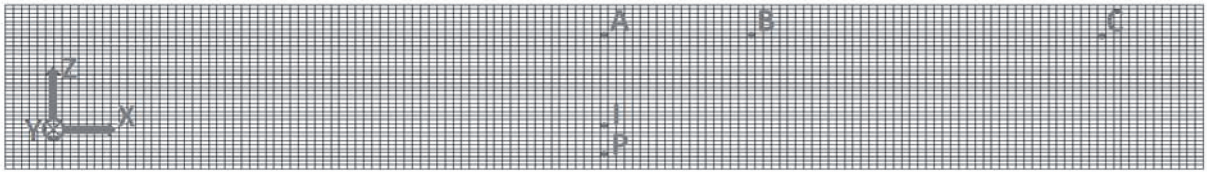

a) Geometry modeling, location of the grid cells for the reservoir simulator with *I* and *P* the cells corresponding to the location of injection and production wells and definition of grid cells *A*, *B* and *C*.

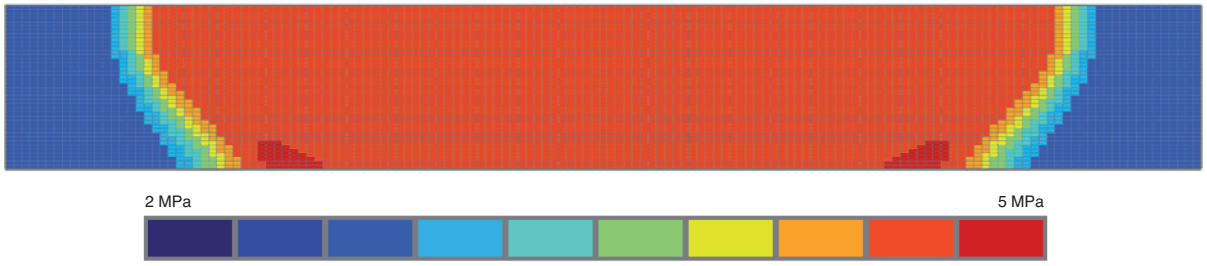

b) Pressure field.

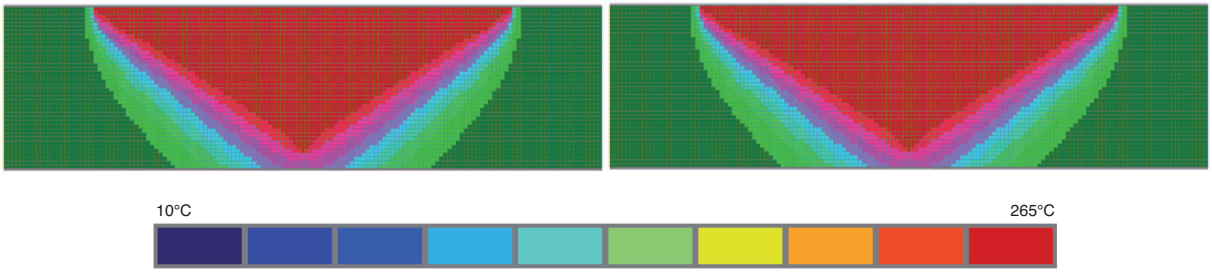

c) Temperature field.

Figure 1

Definition of reservoir simulator spatial a) discretization, b) pressure, c) temperature, fields at the end of simulation (1 500 days) in oil sand reservoir (at 250 m depth).

The iterative coupling between the reservoir simulator and the geomechanical simulator is performed for periods of 5 days. It means that the reservoir permeability and porous volume are corrected 300 times during the simulations.

The evolution of the main variables has been studied in three different grid cells which represent three different zones in the reservoir *(Fig. 2-4)*. These cells are located in the same *X-Z* plane and at the same elevation in the *Z* direction. Figure 1a shows the location of these grid cells (*A*, *B* and *C*). Grid cell *A* is placed just in the middle of the reservoir and 5.5 meters above the injection well. Grid cells *B* and *C* are chosen further from the wells, with the distance of 18.5 and 60 meters from the grid cell *A*, respectively.

Inside the reservoir, we can clearly see the arrival of different fronts (quite visible in *B*). The stress front is followed first by the pore pressure front followed by the temperature front and, at the end, the change in saturation.

The invasion of steam (consisting of at least 70% vapour water with the remainder in the liquid phase) occurs when temperature exceeds 70°C. Oil is first replaced by water and then, by steam when temperature reaches 260°C. Accordingly, in grid cell *B* within the steam chamber the pore space is filled after 1 500 days of steam injection with a mixture of 72% steam vapour, 20% water and 8% oil. Temperature will be about 260°C.

The formation of the steam chamber leads to changes in effective stress, total stress and strain in the reservoir rock that cause permeability modifications (Touhidi-Bagigni, 1998; Dusseault, 2008). Figures 2, 3 and 4 illustrate the changes in vertical (σ_{zz}) and horizontal (σ_{zz} and σ_{yy}) stresses in grid cells *A*, *B* and *C* respectively (compression stress taken positive). The stress state in grid cell *A* is significantly changed when the steam injection starts (after 120 days of pre-heating). The steam injection leads to an increase in temperature and pore pressure around the wells. The vertical total stress starts increasing in grid cell *A* whereas it starts decreasing in grid cells *B* and *C*. This phenomenon can be related to a reversed arching effect. Indeed, the rock expands around the wells because of temperature and pressure changes, leading to a vertical total stress increase around the wells and in grid cell *A*. When the pressure front reaches grid cell *B* (after about 400 days as shown in *Fig. 3*), the total vertical stress in *B* starts to increase. This increase is afterwards enforced with the arrival of the temperature front after about 600 days. At the end of the simulation, the pressure and temperature fronts have not clearly reached grid cell *C*. This is the reason why the total vertical stress decreases only at this grid cell.

The horizontal total stress σ_{zz} in the reservoir clearly increases during steam injection in relation with the lateral boundary conditions adopted in the geomechanical model. The total horizontal stress is changed accordingly except at grid cell *A* (*i.e.* around the wells) at the beginning of steam injection *(Fig. 2)* when the steam chamber lateral extension is small compared to the reservoir width.

The evolution of the other total horizontal stress σ_{xy} is strongly related to the plane strain hypothesis adopted in the geomechanical model; it increases at every stages of production in all grid cells (*A*, *B* and *C*).

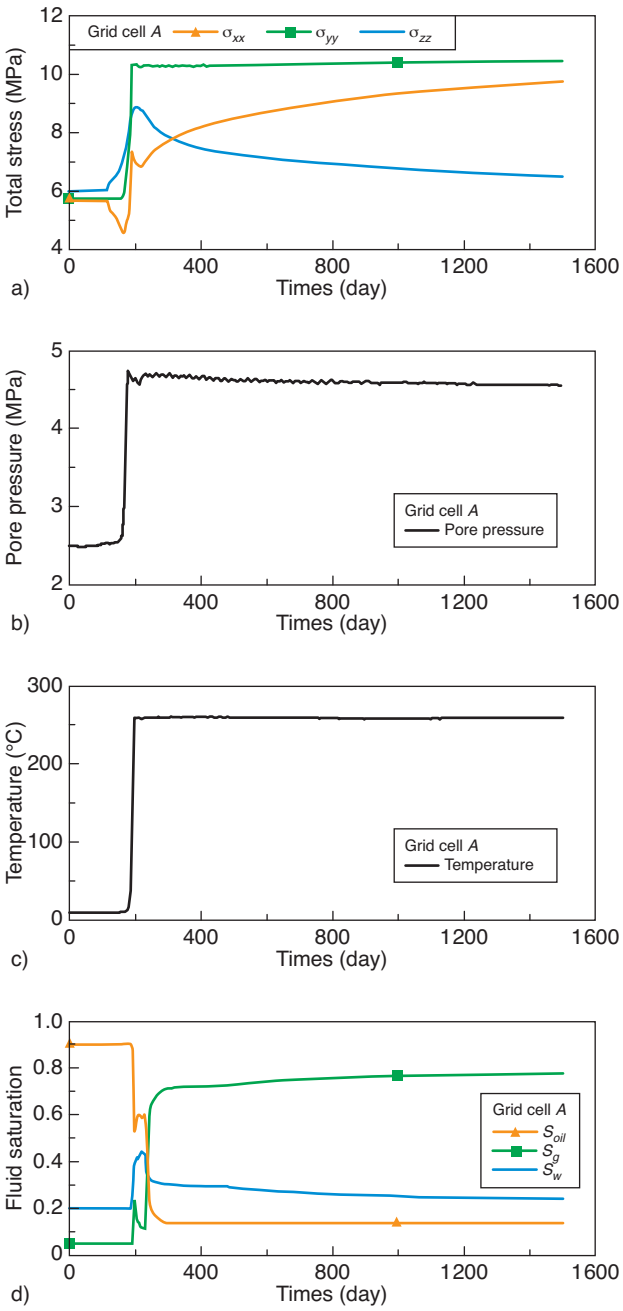

Figure 2

Evolution of total stresses, pore pressure, temperature and pore fluid saturation during simulation at grid cell *A*.

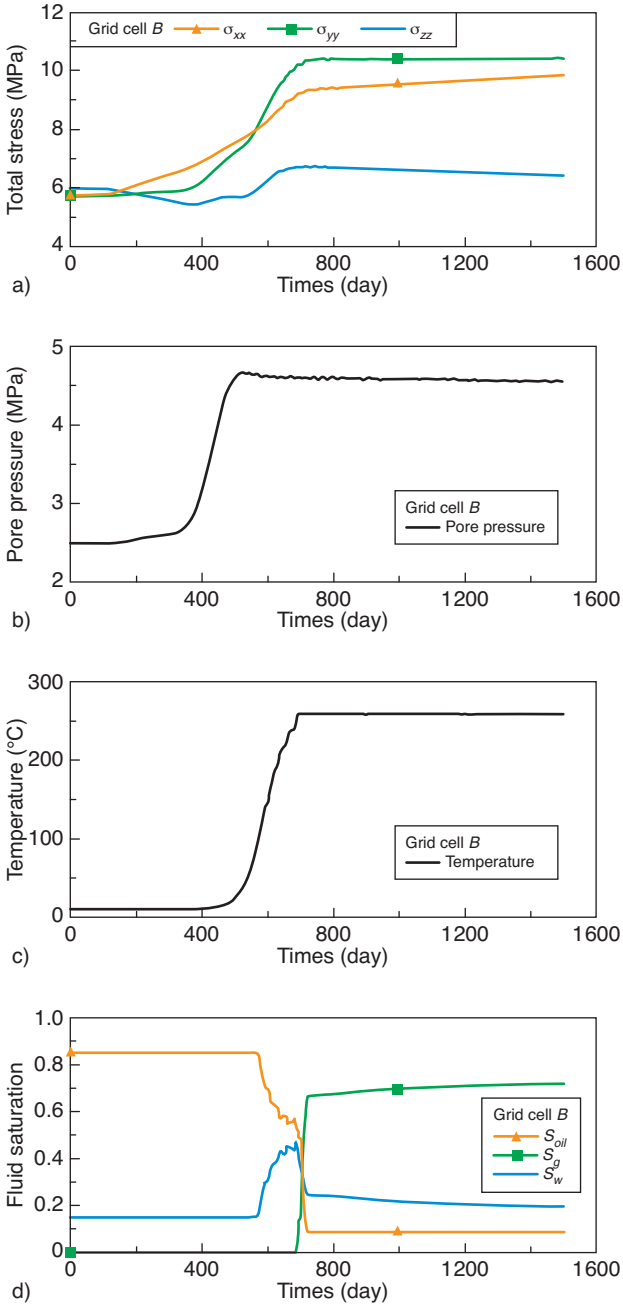

Figure 3

Evolution of total stresses, pore pressure, temperature and pore fluid saturation during simulation at grid cell *B*.

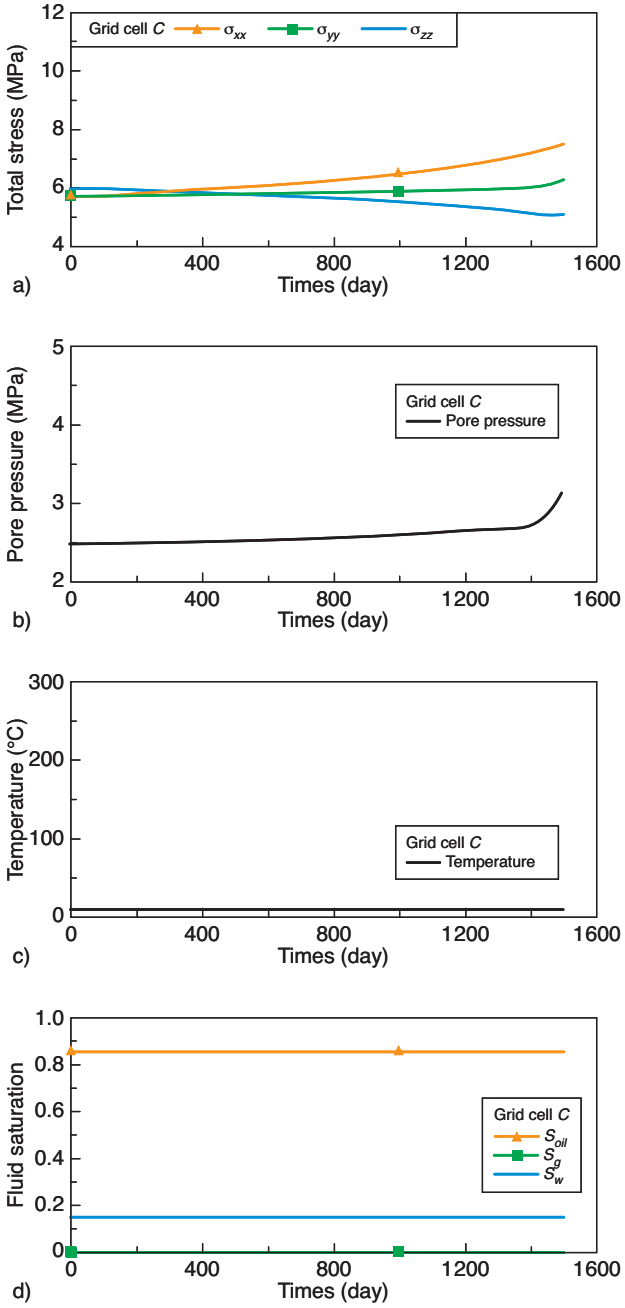

Figure 4

Evolution of total stresses, pore pressure, temperature and pore fluid saturation and during simulation at grid cell *C*.

The results of the geomechanical computation are also presented in a *p'-q* diagram (mean effective stress – deviatoric stress) in Figure 5 for grid cells *A*, *B* and *C*. Considering that the reservoir is confined, two schematic tendencies can be pointed out. For a rock element, firstly, a temperature increase will preferentially lead to an increase of *p'* and to an increase of *q* from an isotropic initial stress state. Secondly, a pore pressure increase will preferentially lead to a decrease of *p'* and an increase of *q* from an isotropic initial stress state.

As shown in Figure 5, the stress path of each grid cell is different, especially far from the steam chamber (grid cell *C*). The same tendency can be observed for grid cells *A* and *B*:

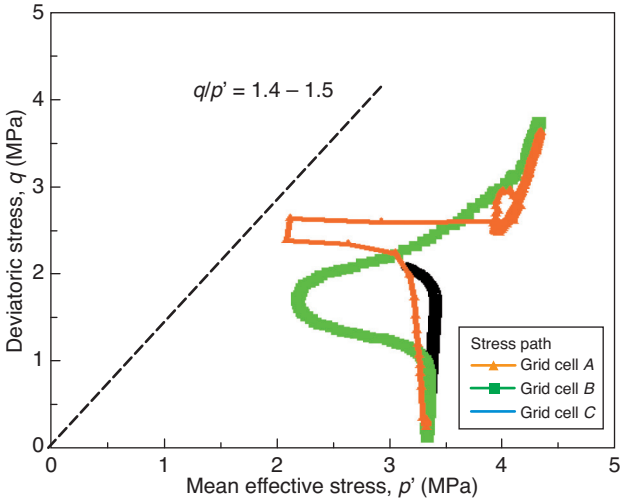

Figure 5

Stress paths in grid cells *A*, *B* and *C* after 1 500 days of simulation.

starting from an isotropic stress state, p' decreases and q increases when the pore pressure front arrives. p' and q afterwards increase when the temperature front arrives. For grid cell *C*, after 1 500 days, the pressure front just arrived with no arrival of the temperature front.

A typical plastic limit characterised by $q/p' = 1.4 – 1.5$ (see Doan, 2011) is also drawn in Figure 5. This plastic limit is close from being reached and it could probably be reached starting from another initial stress state (for example $p' = 2$ MPa and $q = 1$ MPa). The change in both p' and q appear significant, compared to the plastic limit. It should be pointed out that the stress state of grid cells *A* and *B* is closer to the plastic limit once the pore pressure front passed and while the temperature front is arriving.

2 VISCOELASTIC MODEL FOR CANADIAN OIL SAND

The elastic properties of the oil sands depend on the properties of the sand matrix, on the nature of the pore fluid (bitumen, water or steam) and of course on the values of *in situ* stresses and pore pressure. These properties also depend on the frequency of the elastic waves since oil sands are viscoelastic materials.

The approach of Ciz and Shapiro (2007), originally developed for porous rocks saturated with an elastic material, has been used to compute the effective elastic properties of porous rocks filled with various fluids including heavy oil (a viscoelastic fluid with a non negligible shear modulus). This approach reduces to the classical Biot-Gassmann one if the pore fluid is non-viscous in the case of a rock skeleton made up of a single homogeneous mineral.

According to Ciz and Shapiro, the two following equations describe the effective moduli of a sand saturated with a viscous fluid:

$$K_{sat}^{-1} = K_{dr}^{-1} - \frac{(K_{dr}^{-1} - K_s^{-1})^2}{\varphi(K_f^{-1} - K_s^{-1}) + (K_{dr}^{-1} - K_s^{-1})} \quad (2)$$

$$G_{sat}^{-1} = G_{dr}^{-1} - \frac{(G_{dr}^{-1} - G_s^{-1})^2}{\varphi(G_f^{-1} - G_s^{-1}) + (G_{dr}^{-1} - G_s^{-1})} \quad (3)$$

where:

- φ is an uniformly distributed porosity;
- K_{dr}, G_{dr} are the drained bulk and shear moduli ($K_{dr} = K_{dry}$, $G_{dr} = G_{dry}$) of the clean sand (with no oil), respectively;
- K_{sat}, G_{sat} are the effective bulk and shear modulus of the undrained saturated system;
- K_f, G_f are the bulk and shear moduli of saturating fluid;
- K_s, G_s are the moduli of the solid phase.

The sketch of the modeling process is presented in Figure 6.

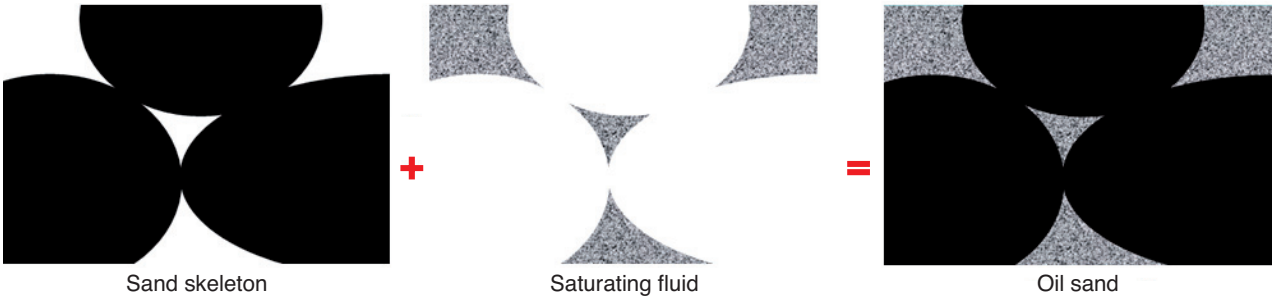

Figure 6

Sketch of modeling process for Canadian oil sand (Ciz and Shapiro, 2007).

2.1 Moduli of the Sand Skeleton

The drained moduli of the unconsolidated or weakly cemented reservoir formation have been widely investigated in the literature. They are independent of the frequency (Spencer *et al*., 1994; Batzle *et al*., 2006a), of temperature (Wang and Nur, 1990; Eastwood, 1993; Batzle *et al*., 2006a; Doan, 2011) and highly stress dependent.

Here, the elastic moduli of the sand skeleton were computed by using a Hertz-Mindlin contact model widely applied in dry granular media. The effective elastic moduli of a dry, dense and random pack of identical elastic spheres is given by (Mavko *et al*., 1998):

$$K_{dr} = \frac{C(1-\varphi)}{12\pi R_g} S_n \tag{4}$$

$$G_{dr} = \frac{C(1-\varphi)}{20\pi R_g}\left(S_n + \frac{3}{2}S_t\right) \tag{5}$$

where C is the average number of contacts per grain (coordination number), R_g is the mean grain radius and φ is the porosity.

Number C was estimated by using the following empirical function $C = 20 - 34\varphi + 14\varphi^2$ (Avseth *et al*., 2010).

S_n, S_t are the normal and tangential stiffness, respectively. The normal stiffness S_n between two identical spheres in the pack under a confining pressure P (Mavko *et al*., 1998; Bachrach *et al*., 2000) is given by:

$$S_n = \frac{4aG_s}{1-\nu_s} \tag{6}$$

The tangential stiffness S_t of two identical spheres under a confining pressure P should be zero if a perfect slip occurs between the spheres. If there is no slip at the contact surface (finite friction), this stiffness is given as (Walton, 1987; Mavko *et al*., 1998):

$$S_t = \frac{8aG_s}{2-\nu_s} \tag{7}$$

where G_s and ν_s are the shear modulus and the Poisson's ratio of the solid grains, respectively, a the radius of the contact area:

$$a = \sqrt[3]{\frac{3FR_c(1-\nu_s)}{8G_s}} \tag{8}$$

where R_c is related to the local radii of curvature of two grains R_1 and R_2 (Bachrach *et al*., 2000); F is a confining force acting between two particles,

$$F = \frac{4\pi R_g^2 P}{C(1-\varphi)} \tag{9}$$

Some particular aspects are to be noted. Firstly, the introduction of parameter R_c (see *Eq. 8)* allows to take into account the grain angularity, a feature clearly observed from microtomography images of Canadian oil sands (Doan, 2011). As quoted by Zimmer *et al*. (2007), the non-spherical shape of sand grains is one of main reason of the difference between empirical and theoretical values. We have assumed $R_c = 0.1 \times R_g$. Secondly, as pointed out by Zimmer *et al*. (2007), the friction between two grains in contact is in reality neither infinite nor zero and the tangential stiffness depends on both the boundary conditions and the loading path (Bachrach and Avseth, 2008). Consequently, one considered here a random case where there are 50% slipping grains and 50% no slipping grains. The Hashin-Strikman average bound has been afterward used to compute the tangential stiffness S_t of the mixture.

2.2 Moduli of the Saturating Fluid

We considered a three-component fluid phase, heavy oil (with saturation S_{oil}), water (with saturation S_w) and gas (S_g). Since there is no gas phase in oil sands under *in situ* conditions (Dusseault, 1980), the introduction of gas occurs as a result of steam injection.

Heavy oils exhibit a viscoelastic behaviour with complex moduli that depend both on frequency and temperature (Batzle *et al*., 2006b; Hinkle, 2008). The Cole-Cole model (see Gurevich *et al*., 2008) was adopted for the complex shear modulus G_{oil}:

$$G_{oil} = G_0 + \frac{G_\infty - G_0}{\frac{1}{(-i\varpi\tau)^\beta} + 1} \tag{10}$$

where G_0 and G_∞ are the shear moduli at zero frequency (very slow deformation) and infinity frequencies (quick deformation), respectively. Exponent $\beta < 1$ is an adjustable parameter. $\tau = \eta/G_\infty$ is the relaxation time and η is the viscosity.

The empirical relationship between viscosity and temperature suggested by Gurevich *et al*. (2008) was used:

$$\ln\left(\frac{\tau}{\tau_\infty}\right) = A.\exp\left(-\frac{T}{T_0}\right) \tag{11}$$

where $\tau_\infty = \eta_\infty G_\infty^{-1}$, T is temperature (°C) and A, T_0 are adjustable parameters.

By default in the model, the viscosity value does not reduce below η_∞. Examination of the changes of heavy oil viscosity curve with respect to temperature provides a minimum viscosity $\eta_\infty = 10^{-3}$ Pa.s

The complex bulk modulus of heavy oil is computed by the following relation (Ciz *et al*., 2009):

$$K_{oil} = K_{ref} + \frac{5}{3} \times G_{oil} \tag{12}$$

where K_{ref} is the bulk modulus of the free non-viscous fluid (K_{ref} = 2.22 GPa).

Ignoring the wetting effect of the mixed fluid phase (oil, water and gas), the overall fluid bulk modulus has been calculated using Ruess average (Mavko *et al*., 1998):

$$\frac{1}{K_f} = \frac{S_{oil}}{K_{oil}} + \frac{S_w}{K_w} + \frac{S_g}{K_g} \quad (13)$$

where K_{oil}, K_w and K_g represent the bulk moduli of the separate phases of oil, water (w) and gas (g) with respective degree of saturations S_{oil}, S_w and S_g.

The overall fluid shear modulus has been calculated using:

$$G_f = G_{oil} \text{ if } S_w + S_g \neq 1 \quad (14)$$

$$G_f = 0 \text{ if } S_w + S_g = 1 \quad (15)$$

The overall fluid density has been calculated using:

$$\rho_f = S_{oil}\rho_{oil} + S_w\rho_w + S_g\rho_g \quad (16)$$

where ρ_{oil}, ρ_w and ρ_g represent the bulk moduli of oil, water (w) and gas (g).

2.3 Calibration of the Model on Laboratory Experiments

Laboratory measurements of *P*- and *S*-waves velocities and attenuations have been performed on natural oil sand samples coming from fluvial-estuarine McMurray sand cores extracted at 75 m below surface from a shallow Athabasca deposit. The *in situ* porosity of the oil sand specimen has been estimated in the range 31-35% from petrophysical log. Oil sands are mostly made of quartz, with grain moduli of K_s = 38 GPa, G_s = 44 GPa and a grain density of 2.65 Mg/m^3.

Velocity measurements have been performed in a pressure cell at 0.5 MHz and in a triaxial cell at 1 MHz under different temperatures (up to 160°C) and isotropic effective stress. Details can be found in Doan *et al*. (2010) and Doan (2011). *In situ* velocities obtained by sonic log measurement (frequency 10 kHz) were also available.

Some main experimental results can be briefly enumerated as follow. *P*- and *S*-wave velocities showed a continuous decrease with increasing temperature. The decrease appeared more pronounced at temperature lower than 60°C. Moreover, velocities gradually increased with increasing confining pressure, as commonly observed in rocks. Sample saturation with a viscous fluid increased both the *P*- and *S*-wave velocities. This can be interpreted not only as a direct consequence of the viscosity effect but also as a result of the viscous contribution to the bulk moduli under saturated conditions.

In addition, our measured high attenuation values on oil sand suggested significant energy losses in the heavy oil sand during the propagation of an acoustic wave. *P*- and *S*-wave attenuations showed a peak as a function of temperature or of the viscosity of the saturating fluid.

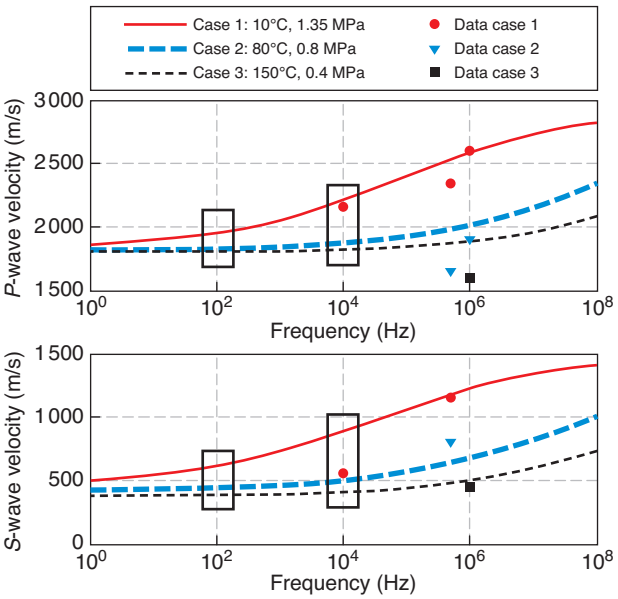

Figure 7

Modeling of velocity dispersion in oil sand. The points around 10^4 Hz represent *in situ* velocities and the points around 10^6 Hz represent our measured data.

These changes in velocity and attenuation reflect the fact that the oil sand is an attenuating and as a consequence, dispersive medium. Therefore, the wave velocities and attenuations depend on the frequency. This is extremely important because laboratory measurements are made at 0.5 or 1 MHz whereas the frequency of the seismic waves used *in situ* are much smaller, around 100 Hz.

The model developed here was used to compute the velocity dispersion in three theoretical cases *(Fig. 7)*. Case 1 corresponds to the initial reservoir conditions (*i.e*. shallow Athabasca reservoirs) in which the temperature is about 10°C and the *in situ* stress about 1.35 MPa (corresponding to a depth of about 75 m). Case 2 (80°C and 0.8 MPa) and case 3 (150°C and 0.4 MPa) correspond to the occurrence of steam injection with increases in temperature and pore pressure. A comparison between the predicted and experimental results (*i.e*. both field velocities and laboratory-measured velocities) *(Fig. 7)* shows a good match, especially for the *P*-wave velocity. It should be noted that the *S*-wave velocity at 10 kHz appeared significantly low in comparison with modeling results, but the very high V_p/V_s (*e.g*. around 3.9) casts doubt on the real value of V_s.

The modeling results showed some other interesting patterns:

– the velocity dispersion (*i.e*. the frequency dependency with respect to velocity) is highlighted at all the conditions of temperature and pressure considered;

– the velocity dispersion curves shift to higher frequencies as temperature increases.

For a fixed frequency *(Fig. 7)*, the predicted velocities considerably change when passing from case 1 (10°C, 1.35 MPa) to case 3 (150°C, 0.4 MPa). At a seismic frequency of about 100 Hz, a decrease of 10% for V_p and of 30% for V_s could be expected. At a sonic frequency of around 10^4 Hz, *P*-wave velocities drop by about 18% and *S*-wave velocities drop up to 44%. Further measurements are needed to check the computed *S*-wave velocities.

3 APPLICATION FOR TIME-LAPSE MONITORING

According to the previous experimental and modeling results, the probable evolution of *P*- and *S*-wave velocities in an oil sand reservoir at seismic frequency bandwidth (*cf.* 100 Hz) at grid cell *B* (located in *Fig. 1*) is illustrated in Figure 8 with respect to the arrival of the different fronts associated to steam injection. The seismic velocities have been calculated by using the Ciz and Shapiro approach, based on input values of pore pressure, temperature and fluid saturation deduced from SAGD coupled thermo-hydro-mechanical modeling.

The arrival of the first front called "stress" is related to a structural effect. As the mean total stress remains constant, it was assumed that the velocities do not change because one only takes into account here the velocity dependence on mean stress. As a consequence, the velocity is assumed isotropic. Further work should be done to include the effect of deviatoric stress changes on velocities. The velocities should probably increase in the direction of the maximum total stress.

When the pore pressure front arrives, velocities V_p and V_s gently decrease, as the mean effective stress decreases.

As the temperature front arrives, the velocities decrease of 10% for compressional waves and of 30% for shear waves. The decrease appears more pronounced below 60°C, levelling off beyond this temperature level. These modeling results are consistent with experimental studies reporting a noticeable change in both velocities at low temperature (cf. below 60°C). Indeed, because the amount of decrease of *S*-wave velocity is relatively larger than that of *P*-wave velocity, the V_p/V_s ratio significantly increases.

The substitution of heavy oil and liquid water by steam (at around 260°C) drastically reduces the compressional velocities V_p with little effect on the shear velocities V_s. The introduction of even a small percentage of gas bubbles into the fluid will have a significant effect on the bulk modulus of the mixture but very little effect on its density *(see Eq. 12, 15)*. The sudden appearance of gas has little effect on V_s due to decreasing density. The V_p/V_s ratio thus drops significantly.

In summary, it is observed that velocities decrease with the steam arrival. These successive changes could be identified by 4D seismic. The sudden appearance of gas is the more influent factor in changing the velocities. It should be pointed out that the evolution of *S*-wave velocities with respect to temperature are relatively more pronounced than that of *P*-wave velocities, suggesting to use the *S*-wave velocities as a indicator of temperature. It should also be noted that at seismic frequencies (up to 100 Hz), most changes in velocities occur at low temperature (below 60°C) with only small

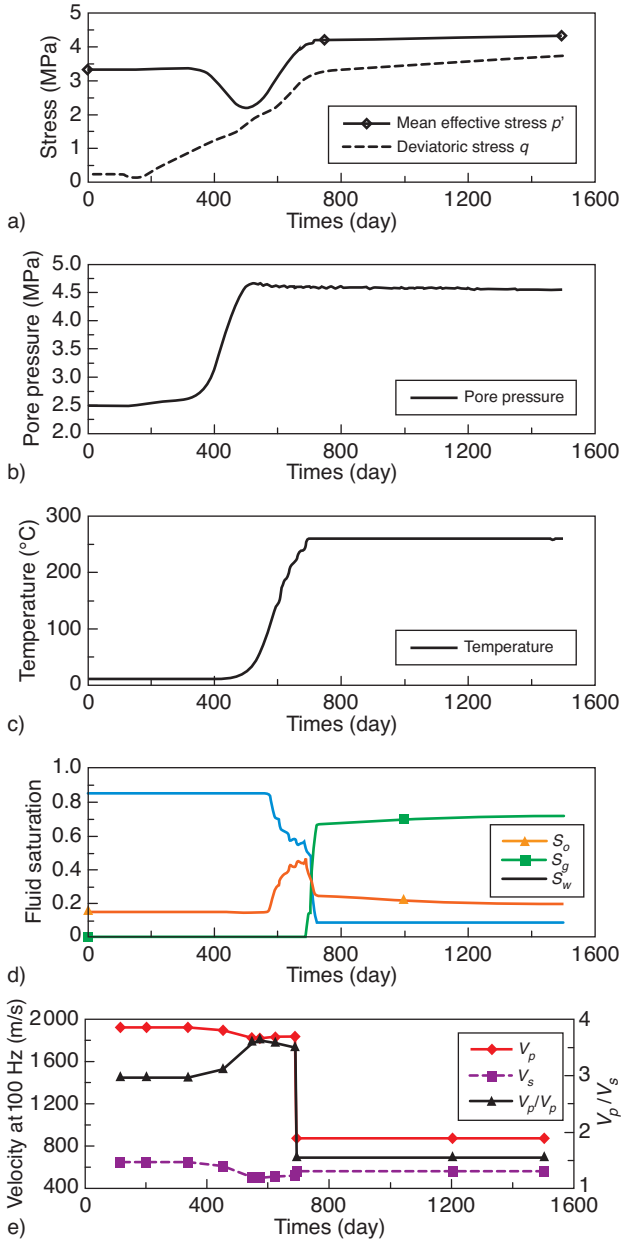

Figure 8

Evolution of the different fields at a typical grid cell (*B*) in an oil sand reservoir (250 m depth).

changes in velocities above this temperature. In other words, one could practically locate the heated zones in the reservoirs but one probably could not deduce the exact temperature of these zones. One would also expect a possible initial decreasing attenuation at seismic frequencies (especially in deep reservoirs) followed by an increasing attenuation during steam injection. However, experimental data to confirm this feature are lacking.

CONCLUSIONS

A coupled thermo-hydro-mechanical modeling of SAGD showed how the different fronts (dilation, pressure, temperature and steam) develop and propagate with respect to time. The invasion of these fronts will impact 4D seismic monitoring because of the changes in seismic attributes (velocities, attenuations, etc.).

The Ciz and Shapiro approach, a generalization of the Biot-Gassmann approach taking into account the viscoelastic behaviour of heavy oil, has been tested to model the oil sand velocity dispersion. The model has been calibrated on the velocities measured in laboratory and *in situ* (before injection). It has then been used to calculate the *P* and *S*-wave velocities in the reservoir at seismic frequency (100 Hz). Until vapour injection, temperature appears to be the dominant factor affecting the wave property response through its dominant effect on the viscosity and the properties of the heavy oil. The sudden appearance or disappearance of gas, if it occurs, is probably the strongest factor in changing the velocities.

ACKNOWLEDGMENTS

The authors would like to thank M. P. Rasolofosaon and M. G. Renard for many useful recommendations and helpful comments.

REFERENCES

Avseth P., Mukerji T., Mavko G., Dvorkin J. (2010) Rock-physics diagnostics of depositional texture, diagenetic alterations, and reservoir heterogeneity in high-porosity siliciclastic sediments and rocks - A review of selected models and suggested work flows, *Geophysics* **75**, 5, 75A31-75A47.

Bachrach R., Avseth P. (2008) Rock physics modeling of unconsolidated sands: Accounting for nonuniform contacts and heterogeneous stress fields in the effective media approximation with applications to hydrocarbon exploration, *Geophysics* **73**, 6, E197-E209.

Bachrach R., Dvorkin J., Nur A.M. (2000) Seismic velocities and Poisson's ratio of shallow unconsolidated sands, *Geophysics* **65**, 559-564.

Batzle M.L., Han D.H., Hofmann R. (2006a) Fluid mobility and frequency-dependent seismic velocity – Direct measurements, *Geophysics* **71**, N1-N9.

Batzle M.L., Hofmann R., Han D.H. (2006b) Heavy oils-seismic properties, *Lead. Edge* **25**, 750-756.

Biot M.A. (1941) General theory of three-dimensional consolidation, *J. Appl. Phys.* **12**, 155-164.

Ciz R., Shapiro S.A. (2007) Generalization of Gassmann equations for porous media saturated with a solid material, *Geophysics* **72**, A75-A79.

Ciz R., Saenger E.H., Gurevich B., Shapiro S.A. (2009) Temperature-dependent poroelastic and viscoelastic effects on microscale-modeling of seismic reflections in heavy oil reservoirs, *Geophys. J. Int.* **176**, 3, 822-832.

Das A., Batzle M. (2008) Modeling studies of heavy oil in between solid and fluid properties, *Lead. Edge* **27**, 1116-1123.

Doan D.H., Nauroy J.F., Delage P., Baroni A., Mainguy M. (2010) Effect of temperature on ultrasonic velocities of unconsolidated sandstones reservoirs during the SAGD recovery process, *Paper in 44th US Rock Mechanics Symposium and 5th U.S.-Canada Rock Mechanics Symposium,* Salt Lake City, 27-30 June.

Doan D.H. (2011) Impact de la température sur les propriétés mécaniques et acoustiques des roches concernées par la production en SAGD, lors de l'injection de vapeur dans les réservoirs d'huile lourde, *Thèse*, École des Ponts ParisTech.

Dusseault M.B. (1980) Sample disturbance in Athabasca oil sand, *J. Can. Pet. Technol.* **19**, 4, 85-92.

Dusseault M.B. (2008) Coupling geomechanics and transport in petroleum engineering, *Proc. SHIRMS International Conference on Geomechanics*, Perth, Australia, 16-19 September.

Eastwood J. (1993) Temperature-dependent propagation of *P*- and *S*-waves in Cold Lake oil sands: Comparison of theory and experiment, *Geophysics* **58**, 863-872.

Gassmann F. (1951) Elastic waves through a packing of spheres, *Geophysics* **16**, 673-685.

Gurevich B., Osypov K., Ciz R., Makarynska D. (2008) Modeling elastic wave velocities and attenuation in rocks saturated with heavy oil, *Geophysics* **73**, E115-E122.

Hinkle A. (2008) Relating chemical and physical properties of heavy oils, *Master Thesis*, Colorado School of Mines.

Kato A., Onozuka S., Nakayama T. (2008) Elastic property changes in a heavy oil reservoir during steam injection, *Lead. Edge* **27**, 1124-1131.

Lerat O., Adjemian F., Baroni A., Etienne G., Renard G., Bathellier E., Forgues E., Aubin F., Euzen T. (2010) Modeling of 4D Seismic Data for the Monitoring of Steam Chamber Growth During the SAGD Process, *J. Can. Pet. Technol.* **49**, 6, 21-30.

Longuemare P., Mainguy M., Lemonnier P., Onaisi A., Gérard C., Koutsabeloulis N. (2002) Geomechanics in Reservoir Simulation: Overview of Coupling Methods and Field Case Study, *Oil Gas Sci. Technol.* **57**, 471-483.

Mavko G., Mukerji T., Dvorkin J. (1998) *The rock physics handbook – Tools for Seismic analysis in porous media*, Cambridge University Press.

Mraz T.J., Rajeshwar K., DuBow J.B. (1982) Thermophysical characterization of oil sands. 2. Acoustic properties, *Fuel* **61**, 3, 240-244.

Nakayama T., Takahashi A., Skinner L., Kato A. (2008) Monitoring an oil-sands reservoir in northwest Alberta using time-lapse 3D seismic and 3D P-SV converted-wave data, *Lead. Edge* **27**, 9, 1158-1175.

Nur A., Tosaya C., Vo-Thanh D. (1984) Seismic monitoring of thermal enhanced oil recovery oil recovery processes, Paper in *54th Ann. Int. Meeting of Society of Exploration Geophysics*, Atlanta, December, pp. 337-340.

Settari A., Mourits F.M. (1998) A Coupled Reservoir and Geomechanical Simulation System, *SPE J.* **3**, 219-226.

Spencer J.W., Cates M.E., Thompson D.D. (1994) Frame moduli of unconsolidated sands and sandstones, *Geophysics* **59**, 1352-1361.

Tanaka M., Endo K., Onozulka S. (2009) Estimation of Steam-Chamber Extent Using 4D Seismic, *Canadian International Petroleum Conference*, Calgary, Alberta, 16-18 June.

Touhidi-Baghini A. (1998) Absolute Permeability of McMurray Formation Oil Sands at Low Confining Stresses, *PhD Thesis*, University of Alberta.

Tosaya C., Nur A., Vo-Thanh D., Da Prat G. (1987) Laboratory seismic methods for remote monitoring of thermal EOR, *SPE Reserv. Eng.* **2**, 235-242.

Walton K. (1987) The effective elastic moduli of a random packing of spheres, *J. Mech. Phys. Solids* **35**, 2, 213-226.

Wang Z., Nur A. (1988) Effect of temperature on wave velocities in sands and sandstone with heavy hydrocarbons, *SPE Reserv. Eng.* **3**, 158-164.

Wang Z., Nur A. (1990) Wave velocities in hydrocarbon-saturated rocks: Experimental results, *Geophysics* **55**, 723-733.

Wang Z., Batzle M.L., Nur A. (1990) Effect of different pore fluids on seismic velocities in rocks, *Can. J. Explor. Geophys.* **26**, 104-112.

Zandi S. (2011) Modélisation des effets géomécaniques de l'injection de vapeur dans les réservoirs de bruts lourds, *Thèse*, École des Mines ParisTech.

Zhang W., Youn S., Doan Q. (2005) Understanding reservoir architectures and steam chamber growth at Christina Lake, Alberta, by using 4D seismic and crosswell seismic imaging *SPE Paper* 97808, presented at the *SPE/PS-CIM/CHOA International Thermal Operations and Heavy Oil Symposium*, Calgary, Alberta, 1-3 November.

Zimmer M.A., Prasad M., Mavko G., Nur A. (2007) Seismic velocities of unconsolidated sands: Part 1 - Pressure trends from 0.1 to 20 MPa, *Geophysics* **72**, 2, E1-E13.

Final manuscript received in June 2012
Published online in January 2013